

# Backaction limits on self-sustained optomechanical oscillations

M. Poot,<sup>1,\*</sup> K. Y. Fong,<sup>1</sup> M. Bagheri,<sup>1</sup> W. H. P. Pernice,<sup>1</sup> and H. X. Tang<sup>1,†</sup>

<sup>1</sup>*Department of Electrical Engineering, Yale University, New Haven, CT 06520, USA*

(Dated: May 25, 2022)

The maximum amplitude of mechanical oscillators coupled to optical cavities are studied both analytically and numerically. The optical backaction on the resonator enables self-sustained oscillations whose limit cycle is set by the dynamic range of the cavity. The maximum attainable amplitude and the phonon generation quantum efficiency of the backaction process are studied for both unresolved and resolved cavities. Quantum efficiencies far exceeding one are found in the resolved sideband regime where the amplitude is low. On the other hand the maximum amplitude is found in the unresolved system. Finally, the role of mechanical nonlinearities is addressed.

PACS numbers: 85.85.+j, 42.50.Wk

## I. INTRODUCTION

Optomechanics is a rapidly growing field in which the interaction between optical cavities and mechanical resonators is studied, see Refs. [1–4] for recent reviews. A lot of interest lies in fundamental questions such as the role of gravity in quantum decoherence, the ultimate limits on position detection, and backaction evasion. These questions might be answered by cooling the mechanical resonator to its ground state. Only very recently this has been achieved using the photon pressure in microwave [5] and optical cavities [6]. Using red detuned light the thermal vibrations of the resonator could be cooled below the zero-point motion, which typically lies in the femtometer range [4]. On the other hand, for practical applications, one would like to have amplitudes as large as possible. This can be achieved with blue detuned light, which amplifies the motion of the resonator. For example, we have recently demonstrated a non-volatile mechanical memory [7] and synchronization of remote mechanical oscillators [8] using the large motion amplitudes generated by the optical backaction of an on-chip racetrack cavity. Large amplitude self-sustained oscillations (SSOs) also enabled the observation of chaotic dynamics [9] and the zero-frequency anomaly [7]. Reaching high amplitude motion is thus important for both technological advances as for fundamental research. Here, we address the question what ultimately limits the maximum amplitude of regenerative oscillations in a cavity-optomechanical system.

Figure 1a shows a schematic of a Fabry-Pérot cavity where one of the mirrors can move, forming an optomechanical resonator. The analysis presented here is not limited to this particular system, but can be applied to any cavity-optomechanical system including racetrack cavities [7], photonic crystal structures [10, 11], and even to microwave-cavity optomechanical systems [12–14]. All these systems have in common that a displace-

ment changes the cavity frequency and thereby the number of photons inside it. This results in a backaction on the mechanical element. In the following, first the cavity-resonator dynamics will be introduced in Sec. II, followed by a study of the appearance of self-sustained oscillations (Sec. III). Section IV shows what happens in the large amplitude regime when the harmonic approximation breaks down. Finally, Secs. V and VI study the quantum efficiency and the role of mechanical nonlinearities respectively.

## II. CAVITY-RESONATOR DYNAMICS

The threshold for the onset of optomechanically-induced SSO is well studied, both experimentally and theoretically [2, 3, 15–20]: For small harmonic motion, the cavity field is only slightly perturbed and the photon number oscillates at the mechanical frequency with an in-phase and a quadrature part as illustrated in Fig. 1b. In this linear regime the cavity response is proportional to the motion amplitude. The quadrature part of the oscillating photon occupation changes the damping rate from its intrinsic value  $\gamma_0$ : For red detuned light the optical backaction increases the total damping rate  $\gamma$ , leading to cooling [21–23]. For blue detuning the damping is reduced and can even become negative, the so-called dynamic instability. In that case the amplitude grows exponentially until it becomes limited by nonlinearities in either the resonator or in the cavity, and the cavity dynamics is strongly perturbed by the oscillator motion (Fig. 1c). The main focus of this work is on the role of the cavity, but the question of how mechanical nonlinearities affect the maximum amplitude will be addressed in Sec. VI.

The coupled equations of motion for the displacement  $u$  of a harmonic oscillator and the optical field inside the cavity  $\sqrt{\hbar\Omega_L}a$  (in the frame rotating at the laser frequency,  $\Omega_L$ ), are [17, 19, 22]:

$$m\ddot{u} = -m\omega_0^2u - m\gamma_0\dot{u} + \hbar g_{OM}n \quad (1)$$

$$\dot{a} = -i(\Delta_0 + g_{OM}u)a - \frac{1}{2}\kappa a + \frac{1}{2}\kappa n_{\max}^{1/2}. \quad (2)$$

\*Electronic address: [menno.poot@yale.edu](mailto:menno.poot@yale.edu)

†Electronic address: [hong.tang@yale.edu](mailto:hong.tang@yale.edu)

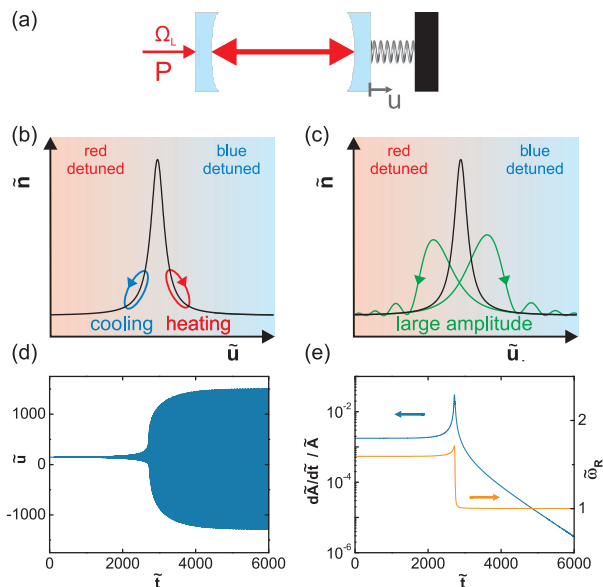


FIG. 1: (Color online) (a) Schematic representation of a generic optomechanical system. Laser light with power  $P$  enters the Fabry-Pérot cavity through the left mirror and bounces back and forth between the two mirrors. The right mirror acts as a mechanical resonator. (b) Optical backaction in the small amplitude limit. A delay between the displacement  $\tilde{u}$  and the change in the photon occupation  $\tilde{n}$  due to the finite cavity lifetime  $\tilde{\kappa}^{-1}$  leads to ellipsoidal trajectories whose area is proportional to the work done on the resonator. Negative (positive) work leads to cooling (heating) of the resonator in the red (blue) detuned region. (c) The optical backaction in the large amplitude regime where the oscillator sweeps across the entire cavity resonance. The black line in (b,c) indicates the position and linewidth of the cavity. (d) Simulated ringup of a mechanical resonator with  $\tilde{\gamma}_0 = 0.001$ , coupled to a cavity with  $\tilde{\kappa} = 100$ ,  $\tilde{\Delta}_0 = 30$ , and  $c_{OM} = 2000$ . From this timetrace the amplification rate  $\tilde{A}^{-1}d\tilde{A}/d\tilde{t}$  and oscillation frequency  $\tilde{\omega}_R$  are derived (e).

Here,  $\omega_0$  and  $m$  are the resonator frequency and mass, and  $n = a^*a$  is the cavity photon number. The detuning is the frequency difference between the laser and the cavity. For zero displacement this is:  $\Delta_0 = \Omega_L - \Omega_c|_{u=0}$ ; a displacement changes this to  $\Delta = \Delta_0 + g_{OM}u$ , where  $g_{OM} \equiv -\partial\Omega_c/\partial u$  is the optomechanical coupling constant. When the detuning is zero, the laser with power  $P$  fills the cavity with photons until the occupation reaches the steady-state value  $n_{\max} = 4P\kappa_c/\kappa^2\hbar\Omega_L$ , where the cavity linewidth  $\kappa$  is the sum of the external and intrinsic linewidths ( $\kappa_c$  and  $\kappa_i$  respectively). Note that for most situations the linear coupling between the cavity frequency and the displacement suffices, but refinements have been proposed. These include a displacement-dependent  $g_{OM}$  [7], quadratic coupling [24], multiple optical resonances [25, 26], and effects due to moving boundaries [27, 28].

The full model (Eqs. 1 and 2) contains 8 parameters, which are not all independent. By writing the model in

a dimensionless form

$$\ddot{\tilde{u}} = -\tilde{u} - \tilde{\gamma}_0\dot{\tilde{u}} + c_{OM}\tilde{a}\tilde{a}^* \quad (3)$$

$$\dot{\tilde{a}} = -i(\tilde{\Delta}_0 + \tilde{u})\tilde{a} - \frac{1}{2}\tilde{\kappa}\tilde{a} + \frac{1}{2}\tilde{\kappa}, \quad (4)$$

the number of independent parameters is reduced to 4 [29]. Here, frequencies have been normalized by  $\omega_0$ , and displacements by the lengthscale  $\omega_0/g_{OM}$ , so that  $\tilde{t} = \omega_0 t$  and  $\tilde{u} = g_{OM}u/\omega_0$ . Furthermore,  $\tilde{\gamma}_0^{-1} = \omega_0/\gamma_0$  is the intrinsic quality factor, and the cavity field is scaled as  $\tilde{a} = a/\sqrt{n_{\max}}$  and  $\tilde{n} = n/n_{\max}$ . The coupling strength is  $c_{OM} = 2n_{\max}u_{zpm}^2g_{OM}^2/\omega_0^2$ , indicating that the coupling can be viewed as the ratio of the zero-point-motion-induced fluctuations of the cavity frequency compared to the resonator frequency. Also note that the optomechanical coupling coefficient  $g_{OM}$  appears in  $c_{OM}$  squared due to the forward- and backaction [4].

Equation 3 can be rewritten in terms of the complex amplitude  $\tilde{U} \equiv (\tilde{u} - i\dot{\tilde{u}})\exp(-i\tilde{t})$  [30] by discarding fast oscillating terms at frequencies  $\sim 2\omega_0$  (the rotating wave approximation):

$$\dot{\tilde{U}} = -\frac{1}{2}\tilde{\gamma}_0\tilde{U} - ic_{OM}\tilde{n}_{\omega_0}, \quad \text{where } \tilde{n}_{\omega_0} = \langle \tilde{n}(t)e^{-i\tilde{t}} \rangle. \quad (5)$$

This describes the evolution of the slowly varying amplitude  $\tilde{A} = |\tilde{U}|$  and phase  $\theta = \angle\tilde{U}$ .  $\tilde{n}_{\omega_0}$  is the Fourier component of the radiation pressure at the oscillation frequency, indicating that only frequencies near the resonance frequency contribute. In the absence of coupling to the cavity (i.e.,  $c_{OM} = 0$ )  $\tilde{A}$  decays exponentially back to zero at a rate  $\frac{1}{2}\tilde{\gamma}_0$ . With coupling present, the out-of-phase part  $-c_{OM}\langle \tilde{n} \sin(\tilde{t} + \theta) \rangle$  of the photon pressure changes the amplitude, whereas the in-phase part  $-c_{OM}\langle \tilde{n} \cos(\tilde{t} + \theta) \rangle$  changes the phase of the oscillations. As explained above, the change in photon number is proportional to a small displacement with some delay. This means that the cavity response can be written as  $\tilde{n}_{\omega_0} = \Phi\tilde{U}$ , where the complex response function  $\Phi$  depends on  $\tilde{\Delta}_0$  and  $\tilde{\kappa}$ . The real part of  $\Phi$  is responsible for the optical spring effect [31, 32] as it changes  $\theta$  at a constant rate. On the other hand, the imaginary part modifies the damping rate from  $\tilde{\gamma}_0$  to  $\tilde{\gamma} = \tilde{\gamma}_0 - 2c_{OM}\text{Im}\Phi$ .

### III. SELF-SUSTAINED OSCILLATIONS

From the discussion in the previous section, it follows that when the imaginary part of  $\Phi$  exceeds  $\tilde{\gamma}_0/2c_{OM}$  the total damping becomes negative and oscillations start to grow exponentially as illustrated in Fig. 1d. Ultimately, the oscillations are limited in amplitude since the power provided by the cavity is finite and the dynamics reaches a limit cycle [29]. This can be understood as follows: when the oscillations become too large,  $\tilde{n}_{\omega_0}$  is no longer linear in  $\tilde{U}$  since the cavity occupation is a nonlinear function of  $u$ , a Lorentzian to be precise. Thus, when the oscillations exceed the range where only the first order term of a Taylor expansion of  $\tilde{n}$  around  $\tilde{u} = 0$  is needed (i.e. it

exceeds the dynamic range), the proportionality between  $\tilde{n}_\omega$  and  $\tilde{U}$  no longer holds, or, equivalently,  $\Phi$  becomes amplitude dependent. An experimental signature of this is the appearance of dips in the optical power coming out of the cavity [7, 15, 16, 33–36] which results when the oscillations sweep past the cavity resonance peak. In principle  $\Phi$  could depend on the complex amplitude at all past times which would make the analysis of the system challenging. However, since the optical cavity field adapts much faster ( $\sim \kappa^{-1}$ ) than the resonator amplitude changes ( $\sim \gamma_0^{-1}$ ),  $\Phi$  only depends on the present amplitude. Moreover, it is independent of the phase of the oscillations,  $\theta$ .  $\Phi$  is thus only a function of  $\tilde{A}$ . Fig. 1e shows the evolution of the amplification rate and the oscillation frequency, which are directly related to the imaginary and real part of  $\Phi$ , respectively. After the transient (Fig. 1d and e) the oscillator reaches a steady state. The backaction-limited amplitude of this limit cycle is a solution to  $\dot{\tilde{A}} = 0$  which is, according to Eq. 5, identical to  $\text{Im}\Phi(\tilde{A}) = \tilde{\gamma}_0/2c_{OM}$ . Note that because the absolute phase  $\theta$  is not fixed, thermal or backaction force noise will lead to a slow phase diffusion of the oscillator [37].

The conclusion of the above discussion is that, to find the maximum amplitude, one needs to know the function  $\Phi(\tilde{A})$ . When the backaction is not too strong and the amplitude is not too high, the motion is to a good approximation harmonic. However, as will be shown in Sec. IV for large amplitudes this is no longer valid and the coupled resonator-cavity dynamics will have to be calculated by numerical integration. The cavity response for  $\tilde{u}(\tilde{t}) = \tilde{A} \cos(\tilde{t})$  was calculated analytically by Marquardt *et al.* [29] as an infinite sum of Bessel functions:

$$\tilde{a}(\tilde{t}) = \frac{\tilde{\kappa}}{2} \sum_{m=-\infty}^{\infty} \frac{J_m(\tilde{A})}{im + i\tilde{\Delta}_0 + \frac{1}{2}\tilde{\kappa}} e^{im\tilde{t} - i\tilde{A} \sin(\tilde{t})}, \quad (6)$$

so that the amplitude-dependent cavity response becomes:

$$\tilde{n}_{\omega_0} = \left(\frac{\tilde{\kappa}}{2}\right)^2 \sum_{m=-\infty}^{\infty} \frac{J_m(\tilde{A})J_{m-1}(\tilde{A})}{(\tilde{\Delta}_0 + m)^2 + (\frac{1}{2}\tilde{\kappa})^2 - (\tilde{\Delta}_0 + m) + \frac{1}{2}i\tilde{\kappa}}. \quad (7)$$

Figure 2 shows the amplitude-dependence of the magnitude and phase of  $\Phi = \tilde{n}_{\omega_0}/\tilde{A}$  for various values of  $\tilde{\kappa}$  ranging from the deeply resolved to the very unresolved sideband regimes. In both regimes, a flat region exists on the left side of the plot where the oscillations of  $n$  are much smaller than  $n_{\text{max}}$  and the cavity response is linear. By taking the limit  $\tilde{A} \rightarrow 0$  of Eq. 7 the cavity response at this plateau is obtained:

$$\Phi(\tilde{A} \rightarrow 0) = -\left(\frac{\tilde{\kappa}}{2}\right)^2 \frac{\tilde{\Delta}_0}{[\tilde{\Delta}_0^2 + (\frac{1}{2}\tilde{\kappa})^2 + \frac{1}{2}i\tilde{\kappa}]^2 - \tilde{\Delta}_0^2}. \quad (8)$$

In the unresolved sideband regime (USR) for large  $\tilde{\kappa}$  (and a constant ratio between  $\tilde{\kappa}$  and  $\tilde{\Delta}_0$ ),  $\Phi(\tilde{A} \rightarrow 0) \propto \tilde{\kappa}^{-1}$ . This is the reason that the plateaus in Fig. 2 collapsed

onto a single curve for the USR. Fig. 2 also shows that the constant region extends up to  $\tilde{A} \sim \tilde{\kappa}$  in the USR; for larger amplitudes the cavity response rolls off smoothly as  $\tilde{A}^{-3}$ .

In the resolved sideband regime (RSR) the situation is different: still there is a constant region at low amplitudes, but the magnitude of  $\tilde{\kappa}\Phi$  now scales as  $\tilde{\kappa}^2$  which also follows from Eq. 8. This can be understood as follows: the cavity linewidth acts as a second-order low pass filter for  $n(t)$  that filters out fast oscillations. The slope of 20 dB/dec means that  $\tilde{A} \sim 1$  is needed to have a response in  $\tilde{n} \sim 1$ . This value of  $\tilde{A}$  thus demarcates the end of the plateau as shown in the Figure. For larger amplitudes,  $\Phi$  is, unlike in the USR, not a smooth function of  $\tilde{A}$ . It contains many dips that become deeper for smaller  $\tilde{\kappa}$  as shown in Fig. 2b. Here, only a few terms contribute to the sum in Eq. 7 which makes the oscillations in the asymptotic form of  $J_m(\tilde{A}) \rightarrow (2/\pi\tilde{A})^{1/2} \cos(\tilde{A} + m\pi/2 + \pi/4)$  for  $\tilde{A} \rightarrow \infty$  apparent. In contrast, in the USR many terms contribute and the oscillations are washed out, resulting in smooth curves.

Since the amplitude of the limit cycle is determined by the condition that the total damping rate is zero ( $\text{Im}\Phi = \tilde{\gamma}_0/2c_{OM}$ , see above) the oscillations of  $\Phi(\tilde{A})$  in the USR lead to a multitude of solutions for the limit cycle of the oscillator for resolved optomechanical systems [29], whereas there is a unique solution for an unresolved system. When expanding the equation of motion for  $\tilde{A}$  (which is obtained from Eq. 5 for small excursions  $\delta\tilde{A}$  around the limit cycle with amplitude  $\tilde{A}$ ) one finds:

$$\dot{\delta\tilde{A}} = -\frac{\gamma_{\tilde{A}}}{2}\delta\tilde{A}, \quad \gamma_{\tilde{A}} = -2c_{OM} \text{Im} \frac{\partial\Phi}{\partial\tilde{A}} \Big|_{\tilde{A}=\tilde{A}} \quad (9)$$

For positive  $\text{Im}[\partial\Phi/\partial\tilde{A}]$  the limit cycle is unstable and the excursions grow until reaching another solution where both the damping rate is zero and where, at the same time, the derivative is negative. Note that even though the limit cycle itself is characterized by a vanishing damping rate  $\tilde{\gamma}(\tilde{A}) = 0$ , perturbations of the oscillator amplitude are overdamped and return to  $\tilde{A}$  at a rate  $\gamma_{\tilde{A}}/2$ . At the fixed point (the limit cycle in the  $u-\dot{u}$  plane corresponds to a fixed point in the  $\tilde{U}$  representation [8]) the oscillation period is  $\omega_0(1 - c_{OM}\text{Re}\Phi)$ , which differs from that of the uncoupled harmonic oscillator due the presence of the nonlinear optical potential [29].

#### IV. THE LARGE AMPLITUDE REGIME

In the discussion above it was assumed that the motion of the oscillator is harmonic during the entire period. This is a good approximation in the RSR, where the cavity cannot respond quickly enough to the fast mechanical oscillations and where the amplitudes are relatively small.

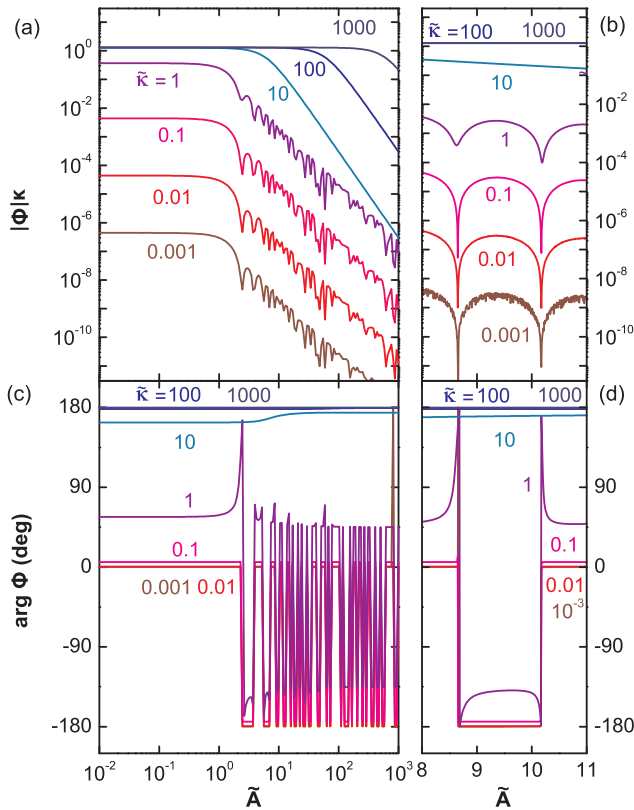


FIG. 2: (Color online) Magnitude (a,b) and phase (c,d) of the steady state response of the cavity photon number  $n_\omega$  to a harmonic displacement with varying amplitude  $\tilde{A}$  for  $\tilde{\Delta}_0 + \langle \dot{u} \rangle = 0.30\tilde{\kappa}$ . The curves with different values for  $\tilde{\kappa}$  are extracted from numerical time-domain simulations (App. A). The right panels show zooms of the area around  $\tilde{A} = 10$ .

On the other hand, in the USR the amplitude will be shown to be much larger and the cavity detuning oscillates back and forth between large negative and positive values. There the photon number thus changes rapidly from zero to a large number and then back to zero. This kicks the resonator every time the detuning crosses zero. When the resonator is moving forward (i.e. to the right in Fig. 1a) work is done on the resonator and the gained energy is transferred back to the cavity during the backward motion. This is also reflected in the dynamics of the oscillator. Instead of the ellipsoidal shape for harmonic motion, Fig. 3a shows a mushroom-like phase portrait with two different amplitudes ( $\tilde{A}_1$  and  $\tilde{A}_2$ ). The step in the velocity coincides with large peaks in  $\tilde{n}$ . Note that both these effects were observed in a optomechanical system consisting of a Bose-Einstein condensate inside a Fabry-Pérot cavity [38]. If the oscillation would sweep through the resonance slowly, the cavity field would always be in equilibrium with the input field and the peaks would have the same height  $n_{\max}$  since  $n(t) = n_{\max}/[\{2\Delta(u(t))/\kappa\}^2 + 1]$ . The work done is then  $\hbar g_{\text{OM}} \int_{-\infty}^{\infty} n(t)v(t) dt = \mp \frac{1}{2}\pi n_{\max} \hbar \kappa$ , where the minus and plus signs are for left and right moving resonators,

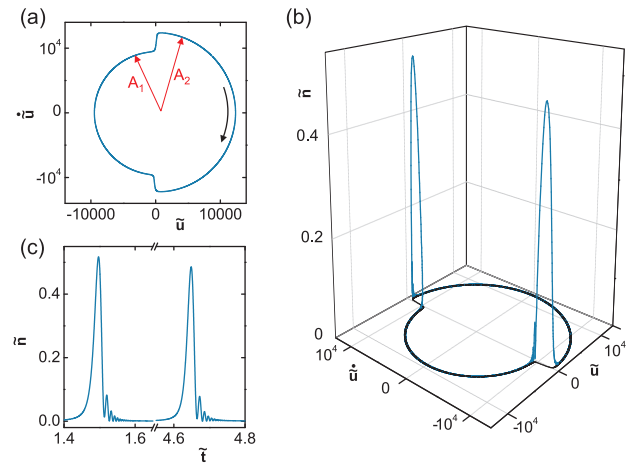


FIG. 3: (Color online) Limit cycles of large amplitude motion in the USR for  $\tilde{\gamma}_0 = 0.01$ ,  $\tilde{\kappa} = 100$ ,  $\tilde{\Delta}_0 = 30$  and  $c_{\text{OM}} = 2 \cdot 10^5$ . (a) Displacement-velocity phase portrait with the two amplitudes ( $A_1$  and  $A_2$ ) and the direction of motion indicated. (b) Three dimensional phase portrait with the photon number on the vertical axis. The black line shows the projection onto the  $\tilde{u}$ - $\dot{\tilde{u}}$  plane. (c) Time trace of the cavity occupation.

respectively. Note that the limits of the integral have been extended to  $\pm\infty$  since long before and long after the resonance is hit, the cavity detuning is so large that the occupation is almost zero at those times. Naturally, the work is proportional to the laser power via  $n_{\max}$  and to the linewidth: a larger  $\kappa$  makes the Lorentzian line-shape wider and hence its area (to which the work is proportional) larger. The work is, however, independent of the optomechanical coupling coefficient since the  $g_{\text{OM}}$ -term in the force  $\hbar g_{\text{OM}} n(t)$  cancels the one originating from the detuning  $\Delta = \Delta_0 + g_{\text{OM}} u$ . More importantly, since the contributions for the left and right moving trajectories are equal, the net work during a whole cycle is zero. Similar to the sideband formalism for *small* motion [17, 22, 23] a delay between the displacement and the cavity response is thus also needed in the large amplitude regime to have the net energy transfer required to overcome the mechanical damping. One effect of such a delayed cavity response is shown in 3b and c. Interestingly, the timetrace of  $\tilde{n}(\tilde{t})$  shows two different peak heights. When the amplitude is small ( $A_1$ ) the velocity is also low and the cavity can fill up for a longer time than during the backward motion with a larger amplitude ( $A_2$ ) and a corresponding larger velocity. Finally, the fast oscillations at the tail of the peaks in Fig. 3c result from interference between the input field and the Doppler-shifted cavity photons that entered the cavity at earlier times [29, 35].

The amplitude of the limit cycle is thus determined by the balance between the net energy gained during one period and the intrinsic damping. Figure 4a shows the maximum amplitude for different coupling strengths plotted against the cavity linewidth. For low coupling

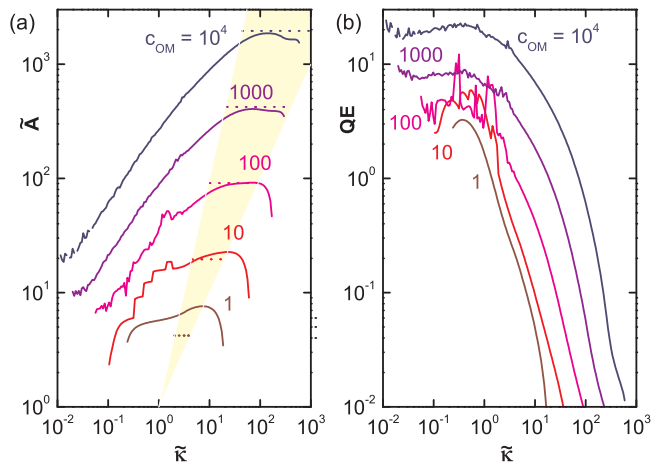


FIG. 4: (Color online) Amplitude (a) and quantum efficiency (b) for  $\tilde{\gamma}_0 = 0.01$  and  $\tilde{\Delta}_0 = 3$ , obtained by direct numerical integration of Eqs. 3 and 4 (see App. A). The dotted lines in (a) indicate the amplitude predicted by Eq. 11 and the shaded region indicates where  $\tilde{A} > \tilde{\kappa}$  and  $\tilde{A} < \tilde{\kappa}^2$  (see text).

the range over which the SSO are stable is narrow, but this increases with increasing  $c_{OM}$ . In the RSR the amplitude is rather small but increases with increasing  $\tilde{\kappa}$ . The timetraces from which Fig. 4 is derived (for details see App. A) show that in the RSR for large coupling ( $c_{OM} \gtrsim 100$ ) the system is chaotic [9]. The scatter of the curves in this regime are reminiscent of this. Also note the multistability of the amplitude in the curve for  $c_{OM} = 10$  [29]. The amplitude keeps on increasing with  $\tilde{\kappa}$  while approaching the USR with an exponent of about  $2/3$ . Then far in the USR the maximum occurs and is finally followed by sharp drop on the right. This divides the region with stable SSO from the one where the out-of-phase part of the backaction is too small to create a negative damping rate.

From the simulations it is clear that the maximum amplitude occurs in the flat region in the unresolved sideband regime. There, the dynamics corresponds to that of Fig. 3 and the first step to analyze the maximum attainable amplitude is to consider the asymmetry in the peaks. For a given initial amplitude, say  $A_1$ , the work done during the kick can be calculated and from that the final amplitude  $A_2$  can be obtained by balancing the difference in work to the mechanical damping [26]. However, even though the peaks have different heights due to the velocity difference, the net work done in one cycle is still zero when accelerations *during* the kick are not taken into account. To proceed, first it is assumed that the kick happens fast so that the displacements before and after are close, which is the case when the time spent within the cavity linewidth is small, i.e.  $\tilde{A}_{1,2} \gg \tilde{\kappa}$ . Secondly, it is assumed that the detuning does not change too fast so that  $\ddot{\Delta}/\tilde{\kappa}^3$ ,  $\dot{\Delta}^2/\tilde{\kappa}^4$  and higher order derivatives are small. This corresponds to  $\tilde{A}_{1,2} \ll \tilde{\kappa}^2$ . The shaded area in Fig. 4a shows that both conditions are satisfied for the flat

region near the maximum amplitude for the larger couplings. The cavity response then becomes:

$$n(\tilde{\Delta}, \dot{\tilde{\Delta}}) \approx \frac{1}{1 + (2\tilde{\Delta}/\tilde{\kappa})^2} \left[ 1 + \frac{32\dot{\tilde{\Delta}}/\tilde{\kappa}^3}{[1 + (2\tilde{\Delta}/\tilde{\kappa})^2]^2} \right], \quad (10)$$

which has the usual Lorentzian shape for adiabatically slow motion that does not yield a net energy transfer, but the second term provides a correction for finite velocity.

When multiplying Eq. 10 by  $\dot{\tilde{\Delta}}$  and integrating over time for both the forward and backward motion, the net energy gain is found. Then by setting this equal to the dissipated energy in one cycle the amplitude  $A^2 = \frac{1}{2}(A_1^2 + A_2^2)$  becomes:

$$A = \left( \frac{3 \hbar^2 g_{OM} n_{\max}^2 Q_0}{4 m^2 \omega_0^3} \right)^{1/3} \quad \text{or} \quad \tilde{A} = \left( \frac{3 c_{OM}^2}{4 \tilde{\gamma}_0} \right)^{1/3}. \quad (11)$$

The dotted lines in Fig. 4a show that the maximum amplitude found from the numerical simulations is indeed given by Eq. 11 when both assumptions are satisfied. For smaller coupling strength the shaded area is narrow and a deviation between the simulated and calculated amplitude develops, indicating that the assumptions break down. However, the simulations show that the amplitude is larger than predicted using Eq. 11, which thus still provides a lower bound. Interestingly, Eq. 11 shows that the amplitude of the oscillations is independent of the cavity decay rate. Although the work done during each kick is  $\propto \tilde{\kappa}$  the net energy transferred does not depend on  $\kappa$  since the latter requires a delay in the cavity response, which is  $\propto 1/\tilde{\kappa}$ . These two contributions thus balance each other. Also  $\tilde{A}$  depends only weakly on the mechanical damping rate  $\tilde{\gamma}_0$  and on the coupling strength  $c_{OM}$ . Yet the largest amplitudes are obtained for the strongest coupling and highest mechanical quality factors. Also, although one needs blue detuning to start the SSOs, the final amplitude is independent of the detuning. This can be understood as follows: when the resonator amplitude is so large that it rapidly sweeps over the cavity and the decay rate is fast enough to empty the cavity before the next kick (c.f. Fig. 3) the exact time at which the kicks happen (as set by the condition  $u(t) = -\Delta_0/g_{OM}$ ) is not really important. Finally, note that the 30 dB/dec slope of  $\Phi$  shown in Fig. 2a is reflected in the exponent of  $1/3$  in Eq. 11.

## V. QUANTUM EFFICIENCY

In the previous section it was shown how to reach the largest amplitudes, however this does not necessarily mean that the process is efficient. The quantum efficiency  $QE$  quantifies how many phonons are generated by a single photon. Semiclassically, it is the ratio of the number of phonons dissipated by the intrinsic damping  $\gamma_0 \times \frac{1}{2} m \omega_0^2 A^2 / \hbar \omega_0$  and the rate of photons entering the cavity  $r_{in}$ . Note that the total rate of photons generated

in the laser  $P/\hbar\Omega_L$  is not used since not all of these photons enter the cavity: this depends on the ratio of  $\kappa_i$  and  $\kappa_c$ . Since the quantum efficiency is an intrinsic property of the cavity-resonator system, only the photons that actually enter the cavity are taken into account. Using Eq. 4 the rate equation for the photon number is found:  $\dot{n} = -\kappa n + r_{in}$ , with  $r_{in}(t) = \kappa n_{\max}^{1/2}(a + a^*)/2$ . The time-dependence of  $r_{in}$  enters via the non-trivial dynamics of  $a$ . However, by averaging over one period of the mechanical resonator and noting that for periodic motion  $\langle \dot{n} \rangle = 0$ , the relation  $\langle r_{in} \rangle = \kappa \bar{n}$  between the average number of phonons in the cavity  $\bar{n}$  and the average rate is obtained. The quantum efficiency then becomes:

$$QE = \frac{\gamma_0}{\kappa \bar{n}} \left( \frac{A}{2u_{z\text{pm}}} \right)^2 = \frac{\tilde{\gamma}_0}{2\tilde{\kappa}c_{OM}} \frac{\tilde{A}^2}{\bar{n}}, \quad (12)$$

where the term in the brackets is identified as the number of phonons in the mechanical resonator. This shows that the larger the amplitude becomes with a smaller average number of photons, the larger  $QE$ .

From the simulated timetraces both the motion amplitude and the average photon number are obtained. Figure 4b shows the dependence of the simulated quantum efficiency for the data shown in panel (a) on the linewidth and coupling strength. In the deeply USR  $QE$  is low because there the cavity can fill up fast and  $n$  is relatively large. The large amplitude reached in this regime thus requires a large amount of photons and the process is not efficient. When decreasing  $\tilde{\kappa}$ ,  $\tilde{A}$  drops (Fig. 4a), but yet the quantum efficiency goes up as  $\bar{n}$  drops faster than  $\tilde{A}^2$ . Finally,  $QE$  saturates to a  $c_{OM}$ -dependent value above 1 when approaching the RSR.

At first it might seem surprising that the quantum efficiency in the RSR can exceed one. Note that this is not an artifact of the definition of  $r_{in}$ : the same holds when using the total laser power. The quantum efficiency is most easily understood using the sideband picture of the optical backaction [1]. Assume that the laser is blue detuned from the cavity by  $\sim \omega_0$ . Photons cannot enter the cavity since their energy is not within the linewidth of the cavity. However, by emitting a phonon the photons end up in the Stokes ( $m = -1$ ) sideband and have the right energy to enter the cavity. This seems to imply that the QE can be at most 1 in the RSR. To understand why QE can be much larger than unity, the sidebands (i.e. Fourier coefficients)  $a_m$  of  $\tilde{a}(\tilde{t})$  are analyzed by expanding the  $\exp(-i\tilde{A}\sin\tilde{t})$  term in Eq. 6, resulting in:

$$a_m \equiv \int_{-\pi}^{\pi} \tilde{a}(\tilde{t}) e^{-im\tilde{t}} d\tilde{t} = \frac{\tilde{\kappa}}{2} \sum_{n=-\infty}^{\infty} \frac{J_n(\tilde{A})J_{n-m}(\tilde{A})}{in + i\tilde{\Delta}_0 + \frac{1}{2}\tilde{\kappa}}. \quad (13)$$

This shows that when  $\tilde{\Delta}_0 \approx 1$  in the RSR a pole occurs for  $n = -1$ . Now for small  $\tilde{A}$  only  $J_0$  and  $J_{\pm 1}$  have an appreciable amplitude, and hence only the  $m = -1$  sideband becomes occupied as illustrated in Fig. 5a. This sideband corresponds to the emission of one phonon whereby the blue-detuned photon ends up at the cavity

resonance. In the USR more values of  $n$  lie within the cavity linewidth and both the  $m = -1$  and  $m = +1$  sidebands are involved in the dynamics (Fig. 5b). The small asymmetry between the Stokes and anti-Stokes sidebands provides the energy to the resonator needed to overcome the intrinsic damping. Also note the difference in amplitudes: In the RSR the carrier ( $m = 0$ ) has a small amplitude as it is detuned from the cavity and the  $m = -1$  sideband is of the same order as the carrier. In the USR the situation is reversed: Now the laser light is within the cavity linewidth and hence the carrier is of order unity, but the sidebands are much smaller. This indicates that the phonon emission efficiency is lower in the USR compared to the RSR.

For small amplitudes there are thus only one or two sidebands, but for large amplitudes the situation is different (Fig. 5c,d): now many more Bessel functions have a nonvanishing value and more sidebands emerge. The number of sidebands can be estimated as follows: the motion of the oscillator frequency modulates the light inside the cavity up and down. Light that entered the cavity at time  $t_0$  becomes frequency shifted by  $g_{OM}[u(t) - u(t_0)]$  at time  $t$ . The number of available sidebands in the RSR is thus roughly equal to the dimensionless amplitude  $\tilde{A}$ . Figure 5c and d show that is indeed the case. In the USR  $a_m$  decays faster than in the RSR due to the shorter lifetime. Finally, the overall quantum efficiency is the balance between the number of available sidebands and the probability to emit a single phonon. The sidebands for small motion in Fig. 5a and b showed that the latter process is very efficient in the RSR but less efficient in the USR, although  $QE$  can still exceed one in the USR for large coupling. Combining all of this indicates that in the RSR the quantum efficiency could be as high as  $QE \sim \tilde{A} \gg 1$ , which is the result of multi-phonon emission. This maximum value is indeed reached just before the end of the SSOs on the left side of Fig. 4a and b.

## VI. OPTICAL VS MECHANICAL NONLINEARITIES

So far only the optical nonlinearities that limit the motion of the self-sustained oscillations have been addressed. Another source of nonlinearity that can limit the amplitude is mechanical in origin: when the motion is large, stress induced in the resonator modifies the resonance frequency from the small displacement value. For moderate amplitudes, the equation of motion becomes that of the well-known Duffing resonator, now combined with optomechanical backaction:

$$\ddot{u} = -\gamma_0 \dot{u} - \omega_0^2 u - \omega_0^2 \alpha u^3 + \hbar g_{OM} n/m. \quad (14)$$

The nonlinearity parameter  $\alpha$  has the units of  $\text{m}^{-2}$  and the scaled version is defined as  $\tilde{\alpha} = \alpha \omega_0^2 / g_{OM}^2$ . A positive value of  $\tilde{\alpha}$  indicates a stiffening mechanical spring, whereas a negative value corresponds to a spring constant

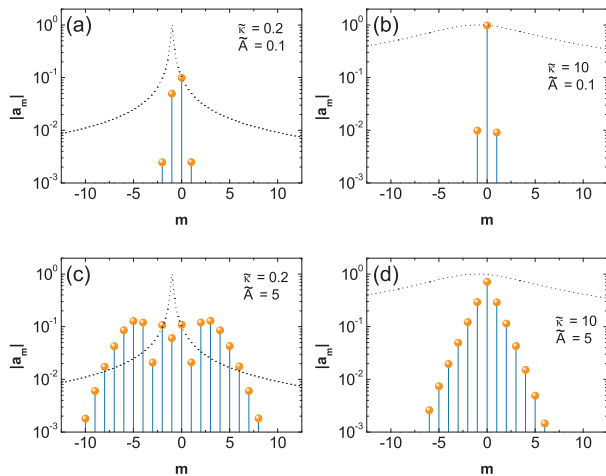


FIG. 5: (Color online) Motion-induced sidebands of the optical field for small (top) and large amplitude (bottom) in the RSR (left) and USR (right). Negative  $m$  corresponds to the emission of phonons, positive  $m$  to absorption. For  $\tilde{\Delta}_0 = +1$  the cavity resonance is located at  $m = -1$  (dotted lines).

that decreases with increasing amplitude. The most important effect of the cubic term in this context is that it modifies the frequency of the oscillations when the amplitude changes. For small  $\tilde{\alpha}$ , the oscillator simply oscillates at the optical-spring-modified resonance frequency. However, when  $\tilde{\alpha}$  is large the oscillation frequency shifts. Figures 6a and b show the oscillation frequency of two nonlinear resonators oscillating due to the optical backaction of an unresolved (a) and a resolved optical cavity (b). In the unresolved case, the oscillation frequency is shifted by almost a factor of two for  $\tilde{\alpha} = 0.002$  compared to the harmonic oscillator. For negative  $\tilde{\alpha}$  the frequency can be lowered to about 90% of the original value before the resonator escapes from the metastable state around  $u = 0$  (see inset). Fig. 6c shows the dependence of the motion amplitude on  $\tilde{\alpha}$ . Although there is a dependence, only a  $\sim 10\%$  change is visible. This is because in the USR the backaction is broadband in nature, and a change in resonance frequency will hardly affect the amplitude of the oscillator. In the RSR the situation is different. Here the laser should be close to the blue sideband of the cavity (i.e., at  $\Delta_0 + g_{OM}\langle u \rangle = \omega_R$ ) to have strong backaction heating. A change in the oscillation frequency with amplitude will move the detuning away from this optimal value and thus reduce the resulting oscillation amplitude. The simulations in Fig. 6d show that this is indeed the case. The oscillation amplitude is strongly peaked around  $\tilde{\alpha} = 0$  and drops when moving away from this value. For large magnitudes of  $\tilde{\alpha}$  the feedback mechanism mentioned above clamps the amplitude to a value of  $\tilde{A} \sim 1$ . Note that this can be used to create a tunable optomechanical oscillator. First the nonlinear resonator is set into oscillation with the optimal  $\tilde{\Delta}_0$ , but then the detuning is slowly adjusted. Since the amplitude is strongly peaked for  $\omega_R = \Delta_0 + g_{OM}\langle u \rangle$

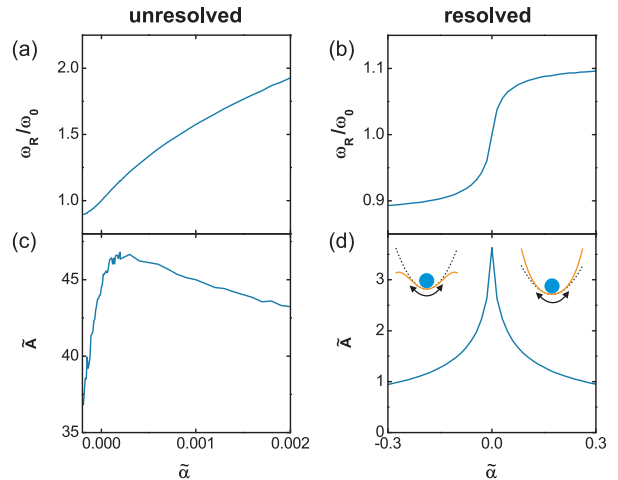


FIG. 6: (Color online) Oscillation frequency (a,b) and amplitude (c,d) of nonlinear resonators in the USR ( $\tilde{\kappa} = 100$ , left) and RSR ( $\tilde{\kappa} = 0.01$ , right) plotted against the nonlinearity parameter  $\tilde{\alpha}$ . Both simulations have been done for  $\tilde{\gamma}_0 = 10^{-5}$ ,  $\tilde{\Delta}_0 + \langle \tilde{u} \rangle = 1$ , and  $c_{OM} = 1$ . The insets show the shape of the mechanical potential energy. For negative  $\tilde{\alpha}$  the springconstant weakens (left), and for  $\tilde{\alpha} > 0$  it stiffens (right).

the oscillator frequency can be dragged along with the detuning, thus creating a widely tunable oscillator.

Finally, it is also possible that the mechanical damping of the resonator changes with amplitude as observed in the experiments of Refs. [39–41]. Since in this case only the damping rate changes and  $\omega_R$  remains constant, this effect can easily be accounted for in the present framework by self-consistently solving for the amplitude using the *average* mechanical damping rate. However, as Eq. 11 shows, the final amplitude depends only weakly on the damping rate of the resonator, so the influence of nonlinear damping on the maximum amplitude is expected to be small.

## VII. CONCLUSIONS

The backaction limits on optomechanical motion have been explored using the amplitude dependent cavity response at the oscillation frequency. Above the threshold self-sustained oscillations grow until the resonator reaches a limit cycle set by the dynamic range of the cavity. The largest amplitudes are obtained with an unresolved cavity, but the highest quantum efficiencies are found in the resolved case. The latter can be much larger than one because many sidebands are involved, resulting in multi-phonon emission. For large amplitudes the motion is anharmonic, and numerical simulations show that the final amplitude is insensitive to the cavity detuning and linewidth. Mechanical nonlinearities only have a modest effect in the unresolved sideband regime, whereas in the resolved case the shift in oscillation frequency due

to anharmonicities can have a strong effect on the amplitude.

### Acknowledgments

M.P. thanks the Netherlands Organization for Scientific Research (NWO) / Marie Curie Cofund Action for support via a Rubicon fellowship. H.X.T. acknowledges support from a Packard Fellowship in Science and Engineering and a career award from National Science Foundation. This work was funded by the DARPA/MTO ORCHID program through a grant from AFOSR. We thank Florian Marquardt for discussions.

### Appendix A: Numerical simulations

Eqs. 1 and 2 are integrated numerically using a fourth order Runge-Kutta algorithm with adaptive step size,

which gives the discretized timetraces of the displacement, velocity, and (complex) cavity amplitude as output. The transients where the oscillator relaxes towards its final amplitude are discarded so that the steady-state oscillations remain. The cavity response  $\Phi(\hat{A})$  (Fig. 2) is found by multiplying the cavity occupation  $n(t)$  by  $\exp(-i\omega_0 t)$  and averaging over many cycles. For the data in Fig. 4 an initial state with a much larger amplitude was used to let the oscillator relax preferentially to the solution with the highest amplitude among the set of stable limit cycles. The amplitude  $\hat{A}$  is obtained by calculating the root-mean-squared value of the displacement and multiplying by  $\sqrt{2}$ . This ensures that the obtained value equals the amplitude for sinusoidal oscillations. An alternative definition where half the difference between the minimum and maximum value of  $u(t)$  is used has almost identical numerical values, but naturally shows more scatter near the chaotic regions.

- 
- [1] T. J. Kippenberg and K. J. Vahala, *Cavity optomechanics: Back-action at the mesoscale*, Science **321**, 1172 (2008).
- [2] F. Marquardt and S. M. Girvin, *Optomechanics*, Physics **2**, 40 (2009).
- [3] I. Favero and K. Karrai, *Optomechanics of deformable optical cavities*, Nat Photon **3**, 201 (2009).
- [4] M. Poot and H. S. van der Zant, *Mechanical systems in the quantum regime*, Phys. Rep. **511**, 273 (2012).
- [5] J. D. Teufel, T. Donner, D. Li, J. W. Harlow, M. S. Allman, K. Cicak, A. J. Sirois, J. D. Whittaker, K. W. Lehnert, and R. W. Simmonds, *Sideband cooling of micro-mechanical motion to the quantum ground state*, Nature **475**, 359 (2011).
- [6] J. Chan, T. P. M. Alegre, A. H. Safavi-Naeini, J. T. Hill, A. Krause, S. Groblacher, M. Aspelmeyer, and O. Painter, *Laser cooling of a nanomechanical oscillator into its quantum ground state*, Nature **478**, 89 (2011).
- [7] M. Bagheri, M. Poot, M. Li, W. P. H. Pernice, and H. X. Tang, *Dynamic manipulation of nanomechanical resonators in the high-amplitude regime and non-volatile mechanical memory operation*, Nat Nano **6**, 726 (2011).
- [8] M. Bagheri, M. Poot, L. Fan, F. Marquardt, and H. X. Tang, *Photonic bus synchronization of remote nanomechanical oscillators*, submitted (2012).
- [9] T. Carmon, M. C. Cross, and K. J. Vahala, *Chaotic Quivering of Micron-Scaled On-Chip Resonators Excited by Centrifugal Optical Pressure*, Phys. Rev. Lett. **98**, 167203 (2007).
- [10] M. Eichenfield, J. Chan, R. M. Camacho, K. J. Vahala, and O. Painter, *Optomechanical crystals*, Nature **462**, 78 (2009).
- [11] X. Sun, J. Zheng, M. Poot, C. W. Wong, and H. X. Tang, *Femtogram Doubly Clamped Nanomechanical Resonators Embedded in a High-Q Two-Dimensional Photonic Crystal Nanocavity*, Nano Letters **12**, 2299 (2012).
- [12] C. A. Regal, J. D. Teufel, and K. W. Lehnert, *Measuring nanomechanical motion with a microwave cavity interferometer*, Nat Phys **4**, 555 (2008).
- [13] T. Rocheleau, T. Ndukum, C. Macklin, J. B. Hertzberg, A. A. Clerk, and K. C. Schwab, *Preparation and detection of a mechanical resonator near the ground state of motion*, Nature **463**, 72 (2010).
- [14] J. D. Teufel, D. Li, M. S. Allman, K. Cicak, A. J. Sirois, J. D. Whittaker, and R. W. Simmonds, *Circuit cavity electromechanics in the strong-coupling regime*, Nature **471**, 204 (2011).
- [15] T. J. Kippenberg, H. Rokhsari, T. Carmon, A. Scherer, and K. J. Vahala, *Analysis of Radiation-Pressure Induced Mechanical Oscillation of an Optical Microcavity*, Phys. Rev. Lett. **95**, 033901 (2005).
- [16] Q. Lin, J. Rosenberg, X. Jiang, K. J. Vahala, and O. Painter, *Mechanical Oscillation and Cooling Actuated by the Optical Gradient Force*, Phys. Rev. Lett. **103**, 103601 (2009).
- [17] T. J. Kippenberg and K. J. Vahala, *Cavity Optomechanics*, Opt. Express **15**, 17172 (2007).
- [18] J. M. Aguirregabiria and L. Bel, *Delay-induced instability in a pendular Fabry-Perot cavity*, Phys. Rev. A **36**, 3768 (1987).
- [19] C. Fabre, M. Pinard, S. Bourzeix, A. Heidmann, E. Giacobino, and S. Reynaud, *Quantum-noise reduction using a cavity with a movable mirror*, Phys. Rev. A **49**, 1337 (1994).
- [20] M. Ludwig, B. Kubala, and F. Marquardt, *The optomechanical instability in the quantum regime*, New Journal of Physics **10**, 095013 (2008).
- [21] S. Mancini, D. Vitali, and P. Tombesi, *Optomechanical Cooling of a Macroscopic Oscillator by Homodyne Feedback*, Phys. Rev. Lett. **80**, 688 (1998).
- [22] F. Marquardt, J. P. Chen, A. A. Clerk, and S. M. Girvin, *Quantum Theory of Cavity-Assisted Sideband Cooling of Mechanical Motion*, Phys. Rev. Lett. **99**, 093902 (pages 4) (2007).



- [23] I. Wilson-Rae, N. Nooshi, W. Zwerger, and T. J. Kippenberg, *Theory of Ground State Cooling of a Mechanical Oscillator Using Dynamical Backaction*, Phys. Rev. Lett. **99**, 093901 (pages 4) (2007).
- [24] J. C. Sankey, C. Yang, B. M. Zwickl, A. M. Jayich, and J. G. E. Harris, *Strong and tunable nonlinear optomechanical coupling in a low-loss system*, Nat Phys **6**, 707 (2010).
- [25] C. Metzger, M. Ludwig, C. Neuenhahn, A. Ortlieb, I. Favero, K. Karrai, and F. Marquardt, *Self-Induced Oscillations in an Optomechanical System Driven by Bolometric Backaction*, Phys. Rev. Lett. **101**, 133903 (2008).
- [26] A. Pai, S. Dhurandhar, P. Hello, and J. Vinet, *Radiation pressure induced instabilities in laser interferometric detectors of gravitational waves*, EUROPEAN PHYSICAL JOURNAL D **8**, 333 (2000).
- [27] C. K. Law, *Interaction between a moving mirror and radiation pressure: A Hamiltonian formulation*, Phys. Rev. A **51**, 2537 (1995).
- [28] A. Xuereb and P. Domokos, *Dynamical scattering models in optomechanics: going beyond the coupled cavities model*, New J. Phys. **14**, 095027 (2012).
- [29] F. Marquardt, J. G. E. Harris, and S. M. Girvin, *Dynamical Multistability Induced by Radiation Pressure in High-Finesse Micromechanical Optical Cavities*, Phys. Rev. Lett. **96**, 103901 (2006).
- [30] G. Heinrich, M. Ludwig, J. Qian, B. Kubala, and F. Marquardt, *Collective Dynamics in Optomechanical Arrays*, Phys. Rev. Lett. **107**, 043603 (2011).
- [31] V. B. Braginsky, S. E. Strigin, and S. P. Vyatchanin, *Parametric oscillatory instability in Fabry-Perot interferometer*, Phys. Lett. A **287**, 331 (2001).
- [32] B. S. Sheard, M. B. Gray, C. M. Mow-Lowry, D. E. McClelland, and S. E. Whitcomb, *Observation and characterization of an optical spring*, Phys. Rev. A **69**, 051801 (2004).
- [33] G. Anetsberger, O. Arcizet, Q. P. Unterreithmeier, R. Riviere, A. Schliesser, E. M. Weig, J. P. Kotthaus, and T. J. Kippenberg, *Near-field cavity optomechanics with nanomechanical oscillators*, Nat Phys **5**, 909 (2009).
- [34] O. Arcizet, P.-F. Cohadon, T. Briant, M. Pinard, and A. Heidmann, *Radiation-pressure cooling and optomechanical instability of a micromirror*, Nature **444**, 71 (2006).
- [35] T. Carmon, H. Rokhsari, L. Yang, T. J. Kippenberg, and K. J. Vahala, *Temporal Behavior of Radiation-Pressure-Induced Vibrations of an Optical Microcavity Phonon Mode*, Phys. Rev. Lett. **94**, 223902 (2005).
- [36] T. Corbitt, D. Ottaway, E. Innerhofer, J. Pelc, and N. Mavalvala, *Measurement of radiation-pressure-induced optomechanical dynamics in a suspended Fabry-Perot cavity*, Phys. Rev. A **74**, 021802 (pages 4) (2006).
- [37] D. A. Rodrigues and A. D. Armour, *Amplitude Noise Suppression in Cavity-Driven Oscillations of a Mechanical Resonator*, Phys. Rev. Lett. **104**, 053601 (2010).
- [38] F. Brennecke, S. Ritter, T. Donner, and T. Esslinger, *Cavity Optomechanics with a Bose-Einstein Condensate*, Science **322**, 235 (2008).
- [39] S. Zaitsev, R. Almog, O. Shtempluck, and E. Buks, in *MEMS, NANO and Smart Systems, 2005. Proceedings. 2005 International Conference on* (2005), pp. 387 – 391.
- [40] S. Zaitsev, O. Shtempluck, E. Buks, and O. Gottlieb, *Nonlinear damping in a micromechanical oscillator*, Nonlinear Dynamics **67**, 859 (2012), 10.1007/s11071-011-0031-5.
- [41] A. Eichler, J. Moser, J. Chaste, M. Zdrojek, I. Wilson-Rae, and A. Bachtold, *Nonlinear damping in mechanical resonators made from carbon nanotubes and graphene*, Nat Nano **6**, 339 (2011).